Optics & Laser Technology 161 (2023) 109174

Contents lists available at ScienceDirect

Optics and Laser Technology

journal homepage: www.elsevier.com/locate/optlastec

Full length article

# Effects of temperature gradient and beam path height from heat source on phase structure and mutual coherence functions of a light beam propagating through convective air turbulence

Ebrahim Mohammadi Razi [a,*], Saifollah Rasouli [b,c,d]

[a] Department of Physics, Faculty of Basic sciences, University of Bojnord, P. O. Box: 1339, Bojnord, Iran
[b] Department of Physics, Institute of Advanced Studies in Basic Sciences, P. O. Box: 45195-1159, Zanjan, Iran
[c] Optics Research Center, Institute for Advanced Studies in Basic Sciences, P. O. Box: 45195-1159, Zanjan, Iran
[d] The Abdus Salam ICTP, Strada Costiera 11, Trieste 34151, Italy

ARTICLE INFO

*Keywords:*
Phase structure function
Mutual coherence function
Non-Kolmogorov turbulence
Anisotropic turbulence

ABSTRACT

In this paper, we investigate the effects of different values of temperature gradient (TG) and the distance of a plane wave path from a flat heat source generating an anisotropic and non-Kolmogorov convective air turbulence medium on the phase structure function (PSF) and mutual coherence function (MCF) of the light beam propagating through the medium. The non-Kolmogorov and anisotropic convective air turbulence is created using an electrical heater with a surface size of 50 cm × 100 cm. The heater temperature is changeable from room temperature to 100 °C. The laser beam with a diameter of 20 cm passes through the turbulent medium at different distances from the heater surface. At the end of the path, the wavefront of the light beam is reconstructed using a two-channel moiré wavefront sensor. Then, the PSF and MCF are calculated, and the effects of different TGs and the different beam path heights from the heater are studied. Results show that with increasing the TG and decreasing the beam path distance from the heat source, the turbulence intensity and PSF increase, while the MCF decreases.

## 1. Introduction

Atmospheric turbulence has been studied for a long time. However, many aspects of the turbulent medium and its effects on light beam propagation through the medium are still not fully understood. This incomplete identification is due to the complexity of the underlying equation of motion, and the inability of a numerical simulation of a real turbulent condition. Since the invention of the laser beam, studying the effects of the atmospheric turbulence on the characteristics of a laser beam that propagates through it has also been a fascinating subject. Various models have been proposed for turbulence study, among which the Kolmogorov model is a common one; it is based on the homogeneity and isotropy of the turbulence. Many studies show that atmospheric turbulence is non-Kolmogorov [1–9] and anisotropic [10–18]. Most features of the light beam such as intensity [19–22], wavefront form [17,18,23–26], polarization [27–29], spot size [30–32] and coherence function [33–36] vary during propagation through the atmospheric turbulence. The light coherence is an important factor for many applications, including imaging [37], tomography [35,36], and free-space optical communication [38–43]. The coherence function may be measured via various methods such as interferometry [33,44], 2- and 4-differential images motion monitoring (DIMM) [15,45] and wavefront sensing [25,46].

To the best of our knowledge, there has been no comprehensive study on the effect of a temperature gradient (TG) on the statistical properties of the phase structure function (PSF) and mutual coherence function (MCF) of a light beam wavefront. In this work, we experimentally study the effects of different TGs and the distances of the beam path from the heat source on the PSF and MCF of a light beam propagating through non-Kolmogorov and anisotropic indoor convective air turbulence using a two-channel moiré wavefront sensor. Theoretical examination of the results is a topic that we intend to do in the future.

It is worth mentioning that in three other works where the same setup were used, the effect of the source temperature on the statistical behavior of convective air turbulence [14], the beam wavefront annular Zernike polynomials behavior [17] and anisotropy and scaling of the phase structure function [18] were investigated. Therefore, we omit to mention the advantage of the used setup here, and encourage the readers to find more details in Ref. [18].

* Corresponding author.
*E-mail addresses:* e.mohammadi@ub.ac.ir (E.M. Razi), rasouli@iasbs.ac.ir (S. Rasouli).

https://doi.org/10.1016/j.optlastec.2023.109174
Received 12 August 2022; Received in revised form 10 December 2022; Accepted 10 January 2023
Available online 17 January 2023

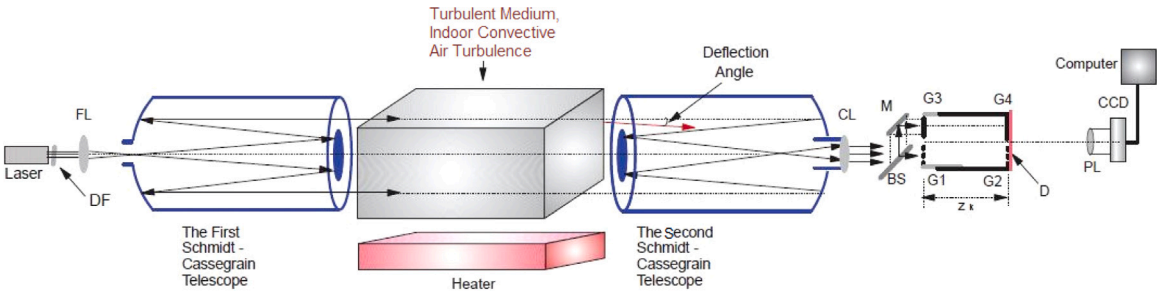


**Fig. 1.** Schematic diagram of the experimental setup. $DF$, $FL$, $CL$, $BS$, $M$, $D$, and $PL$ are the neutral density filter, focusing lens, collimating lens, beam splitter, mirror, diffuser, and projecting lens, respectively. $G1$ to $G4$ stand for the gratings.

## 2. Experiments

Experimental works were done in the moiré technique laboratory of the Institute for Advanced Studies in Basic Sciences (IASBS). Fig. 1 shows a schematic diagram of the experimental setup used in this work. Through the first telescope (a 14 inch Celestron Schmidt–Cassegrain telescope), the second harmonic of an Nd-YAG laser with 532 nm wavelength, a diameter of 20 cm, and plane wavefront enters convective air turbulence. An electrical heater with an upper surface having dimensions of 50 cm × 100 cm and the adjustable temperature has been used to create a TG as well as convective air turbulence, which is similar to near-ground turbulence. The effects of the turbulent medium on the light beam were studied by measuring the fluctuations of the wavefront's phase. At the end of the path with 150 cm apart, the light beam is received by the second telescope (a Meade 8 inch LX200 GPS Schmidt–Cassegrain telescope). After passing a positive lens, the light beam is re-collimated and enters a two-channel moiré wavefront sensor with a smaller diameter. Each channel of the wavefront sensor consists of a moiré deflectometer. Directions of the grating rulings were almost parallel in each moiré deflectometer but were perpendicular in the two channels. In the experimental setup shown in Fig. 1, G2 and G4 were installed at a distance of $z_k = 37.5$ cm from G1 and G3, respectively. All the gratings were identical and had a ruling period of 0.1 mm. Moiré patterns were formed on a plane where the second gratings of the moiré deflectometers and a diffuser were installed. The moiré patterns from both channels are projected onto a CCD camera using a projecting lens. For a displacement of the self-image in a direction normal to the grating rulings, moiré fringes were shifted in a direction normal to the moiré fringes direction. The deformation of the moiré fringes caused by the turbulence can be measured by tracing the imaged moiré fringes. Successive moiré patterns are recorded by the CCD camera and transferred to a computer, to allow temporal fluctuations of the wavefront phase to be measured with a high accuracy. Displacements of the moiré fringes in the recorded patterns correspond to the fluctuations of two orthogonal components of the angle of arrival (AA) across the wavefront. Based on the sensor data, the wavefront of the light beam at the entrance aperture of the second telescope is reconstructed. The details of the wavefront reconstruction are fully explained in Refs. [17,18,25].

In comparison with a Shack–Hartmann wave front sensor [47], the two-channel moiré deflectometry-based wave front sensor used here is relatively low cost, high resolution, and adjustable. For instance, the sensor gratings can be easily designed with simple computer software and can be printed on a transparent plastic sheet with a commercial printer. This sensor offers some flexibility, since its dynamic range and sensitivity are adjustable by merely changing the separation of the gratings and the angle between the rulings of the gratings in both channels, respectively. The spatial resolution of the wave front sensing is adjustable by means of bright, dark, and virtual traces for given moiré fringes with no cost in measurement precision. Moiré-based two-channel wave front sensor can even detect the presence of optical vortices on the wave front that might be generated in a highly turbulent condition [48]. Its main drawback for the wave front sensing is the need for a high-level intensity beam, and, therefore, for low light applications as one would normally expect in astronomy, highly sensitive detectors are required. However, to decrease the energy loss, moiré deflectometers can be setup with phase gratings.

To investigate the effect of different TGs, and the beam path distance from the heat source, we allow the light beam propagates in the medium at the altitudes of 13 cm, 30 cm, 80 cm, and 200 cm from the heater surface. For each of the beam path altitudes, the heater temperature was varied from the room temperature to 100 °C with steps 10 °C. At each temperature, a collection of 3000 images were recorded by a charge-coupled device (CCD) camera whose frame rate and exposure time were set to 30 fps and 1 ms, respectively.

## 3. Results and discussion

### 3.1. Phase structure function (PSF)

Complex amplitude of a light beam is given by [49]

$$\psi_z(r) = |\psi_z(r)|\, e^{i\phi_z(r)}, \tag{1}$$

where $z$, $r$, and $\phi_z$ are the distance from the beam source along the propagation direction, the separation distance between two points on the wavefront, and wavefront phase at a distance $z$, respectively. The PSF is defined as phase variance between two separate points on the wavefront and is obtained by [49]

$$D_\phi(r) = \left\langle |\phi(R) - \phi(R+r)|^2 \right\rangle, \tag{2}$$

where the angle brackets $\langle ... \rangle$ denote an ensemble average.

To investigate the isotropy of a turbulent medium, the PSF of the light beam propagating through it, is calculated in two directions, parallel and perpendicular to the heater surface, denoted by $x$ and $y$, respectively. Although understanding the nature of anisotropy requires determining the behavior of PSF in all directions, comparison the PSF measured in two directions, parallel and perpendicular to the heater surface seems to be enough to demonstrate the anisotropy of medium. In addition, we believe that the two-dimensional TGs created in the turbulent medium cause the anisotropy, therefore, PSF has been studied only in two dimensions. As there is a distance between the beam path and the heat source, and due to the limited width of the heater, different vertical and horizontal TGs appeared. The different TGs in $x$ and $y$ directions were measured by at least three digital thermometers. The thermometers were located along vertical and horizontal directions. The measured values of TG in the vertical direction are greater than those in the horizontal direction. Fig. 2 shows calculated PSFs for different distances of the beam path from the heater surface in two directions and different heater temperatures.

In PSF curves illustrated in Fig. 2, two regions are distinct. In the first region for the lower values of the separation of the points, the values of PSFs increase linearly, while in the second region, PSFs are almost saturated. As can be seen from the figure, at a typical

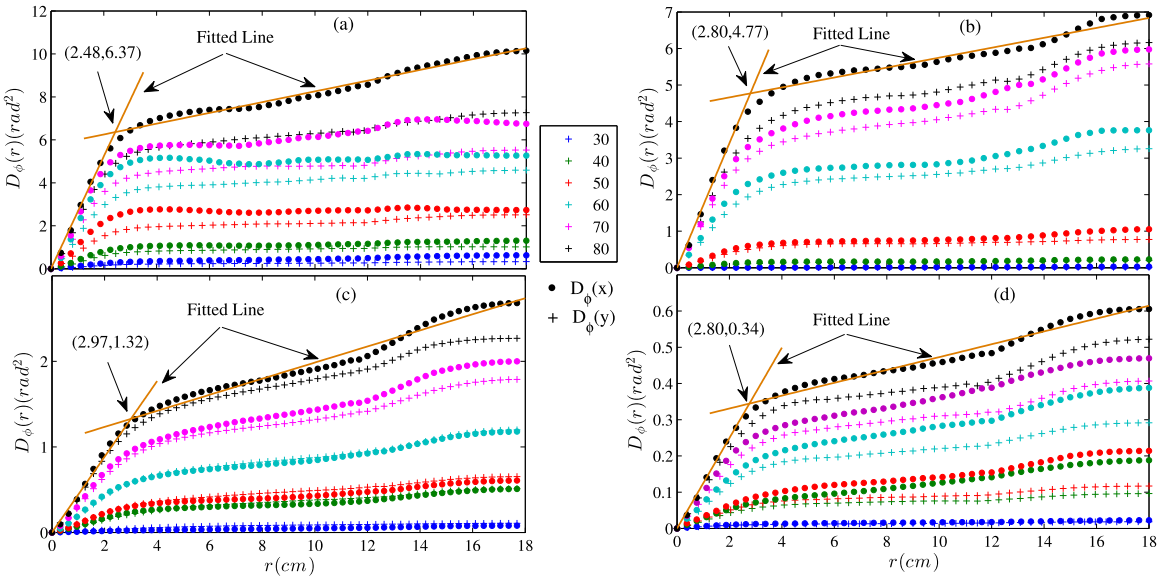


**Fig. 2.** Calculated PSFs for different vertical and horizontal separations of two points at different heater temperatures, based on the reconstructed wavefront over the second telescope's entrance aperture. The beam path distance from the heater's surface was (a) 13 cm, (b) 30 cm, (c) 80 cm, and (d) 200 cm.

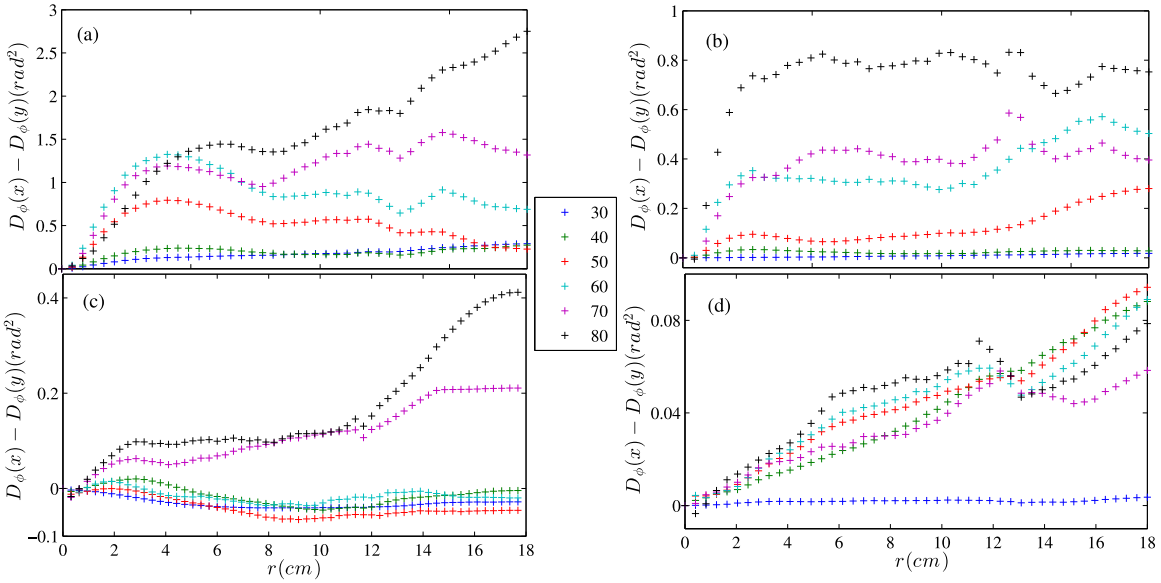


**Fig. 3.** Differences in the measured PSFs for the vertical and horizontal separation of the points. Plots were obtained using the data depicted in Fig. 2.

heater temperature of 80 °C, which is indicated by the black circles in the subplots, the slope of the PSFs is remarkably decreased after separation distance $r$ with values of 2.48, 2.80, 2.97, and 2.80 cm for the beam path distance from the heater's surface of 13 cm, 30 cm, 80 cm, and 200 cm, respectively. The values of PSFs, at those points, are 6.37, 4.77, 1.32, and 0.34 (rad$^2$), respectively. In the saturation region, the PSF values in both directions increase with increasing the heater temperature and decreasing the distance from the heater. The PSF values in this region are related to the turbulence intensity. In other words, the turbulence intensity is stronger at higher heater temperatures and shorter distances from the heater. Another result can be revealed from comparing PSFs of the same beam path height from the heater surface. As is seen, for the lower heater temperatures, the saturation behavior starts at shorter separation distances, $r$. Moreover, at each height from the heater surface and for each temperature, the PSF in two directions are not equal. This result indicates that the turbulence in the presence of the generated TG is anisotropic. For better visualization of the anisotropy, the differences between PSFs in $x$ and $y$ directions for different heater temperatures and different beam path distances from the heater's surface are shown in Fig. 3. As is seen, for the light beam propagating through the layers closed to the heater surface, the difference between PSFs in two directions increases, and as a result, these layers show strong anisotropy. On the other hand, for higher heater temperatures and shorter distances from it, the anisotropy is stronger. Most of the models already used to study turbulence, including Kolmogorov one, are based on their homogeneity and isotropy in the inertial range, say the range between inner and outer scales of the turbulence. The PSF increases linearly in the inertial range. Based on comparing the PSFs in two directions at each heater temperature, the convective air turbulence is anisotropic even in the inertial range. In Ref. [18], by calculating the slope of the PSF curve in the inertial range, it was revealed that the turbulence does not follow the Kolmogorov model when the beam path distance from the heater surface was 80 cm. Here, we see that the same result can be obtained for the distances of 13 cm, 30 cm, and 200 cm for the beam path from the heater surface.

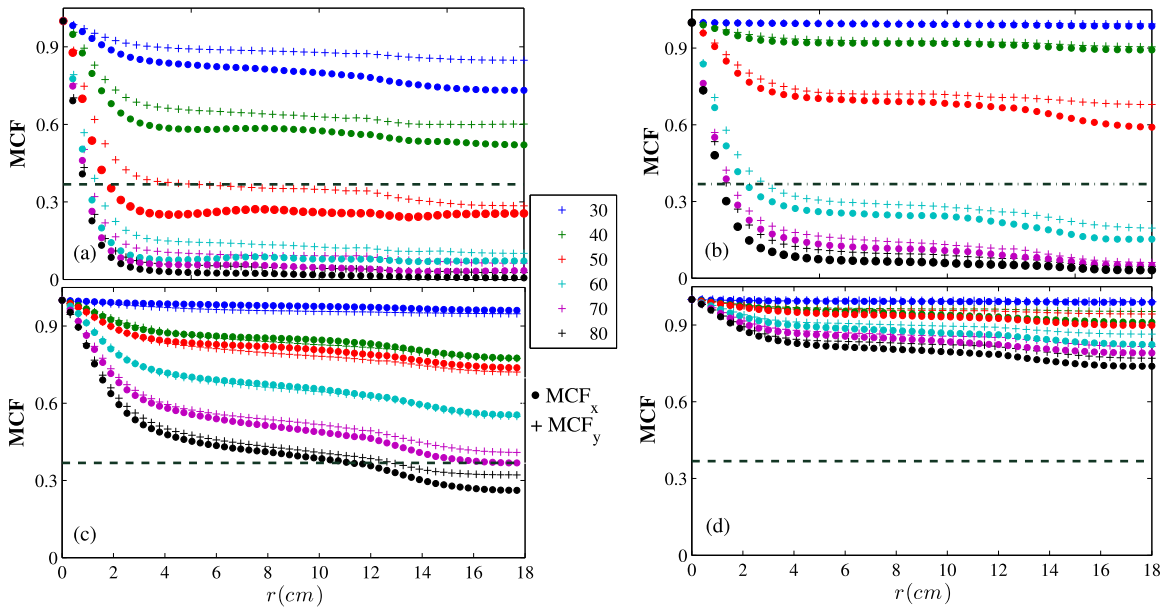


**Fig. 4.** Calculated MCFs for the light beam in vertical and horizontal directions based on the data presented in Fig. 2.

As mentioned earlier, the atmospheric turbulent environment in the layers near Earth's surface is a convective turbulent. According to the results of this section, it can be conclude that the atmospheric turbulence at lower layers behaves as an anisotropic and non-Kolmogorov turbulence [12,15]. Therefore in the studying of light beam propagation through layers near Earth surface non-Kolmogorov and anisotropic model(s) must be used.

### 3.2. Mutual coherence function (MCF)

When a light beam passes through turbulent medium, its degree of spatial and temporal coherence function decreases. The MCF of a light beam is defined as

$$\begin{aligned} MCF(r) &= \langle \psi(r_1)\psi^*(r_2)\rangle, \\ \psi(r_1) &= e^{i\phi(r_1)}, \quad \psi(r_2) = e^{i\phi(r_2)}, \\ MCF(r) &= \left\langle e^{i(\phi(r_1)-\phi(r_2))}\right\rangle, \end{aligned} \tag{3}$$

where $r = r_2 - r_1$ is the separation distance between two points over the wavefront.

Since $\phi(r)$ is the sum of a large number of independent variables, it has a Gaussian statistics with zero mean value. Therefore, MCF can be rewritten as [49]

$$\begin{aligned} MCF(r) &= e^{\frac{-1}{2}\left\langle |\phi(r_1)-\phi(r_2)|^2\right\rangle}, \\ MCF(r) &= e^{\frac{-1}{2}D_\phi(r)}. \end{aligned} \tag{4}$$

Using the measured PSF values in Eq. (4), MCFs are calculated, and presented in Fig. 4. As is seen, for all heater temperatures and all distances from the heat source, the values of MCFs decrease with separation distance between the points, $r$. Moreover, MCF decreases more rapidly for the higher heater temperatures. As mentioned above, a high heater temperature causes an increment in the turbulence intensity, which in turn causes eddies to break to smaller sizes. Propagation of laser beam through the medium, including small eddies, causes further fluctuations of the wavefront, which in turn causes a reduction of the spatial coherence of the laser beam. The coherence radius is the separation distance, $r_c = r$, at which the degree of MCF falls to $e^{-1}$. To better visualization, a dashed line for MCF = $e^{-1}$ is also plotted in Fig. 4. As is seen in Fig. 4(c) and (d), for the low heater temperatures (less than 50 °C) and long distances of the beam path from the heater's surface (80 cm and 200 cm), the value of MCF does not significantly decrease. In contrast, for the higher heater temperatures and shorter distances from the heat source (Fig. 4(a) and (b)), the MCF exhibits a relatively rapid reduction. The beam coherence radius at 80 °C for the distances of 13 cm, 30 cm and 80 cm are determined as 0.7 cm, 1.8 cm and 11 cm, respectively. The MCF does not reach to $e^{-1}$ in the range of 0–18 cm for the distance of 200 cm.

In Ref. [18], by fitting different models to the calculated PSF data from the experimentally measured wavefront gradients, it was revealed that the von Kármán model has the best fit to the experimental data, because it has the lowest mean square error and is fitted in a large range than the other models. For the separation values of the points on the wavefront larger than 12 cm, there was no a good consistency between the experimental data and the considered models. Similarly, in this work, we have investigated the correlation between the experimental data for MCF and various turbulence models which are defined as follows:

- The Tatarskii and the Kolmogorov MCF [49]:

$$MCF^T(r) = exp\left[-\frac{1}{2}\left(6.88(r/r_0)^{5/3}\right)\right], \tag{5}$$

  where $r_0$ is Fried's seening parameter.
- The Gaussian MCF [50]:

$$MCF^G(r) = exp\left[-\frac{1}{2}\left(0.391C_n^2k^2L\chi_G^{-5/3}\{1-exp[-(r^2/r_0^2)]\}\right)\right], \tag{6}$$

  where $k = \frac{2\pi}{\lambda}$, $\chi_G = \frac{2\pi}{L_0}$ and $L$ is the propagating beam length. $L_0$ is the outer scale of turbulence, and $\lambda$ is wavelength.
- The von Kármán MCF [50]:

$$MCF^K(r) = exp\left[-\frac{1}{2}\left(0.391C_n^2k^2L\chi_K^{-5/3}[1-\frac{2^{\frac{1}{6}}}{\Gamma(\frac{5}{6})}(\chi_K r)^{\frac{5}{6}}K_{\frac{5}{6}}(\chi_K r)]\right)\right], \tag{7}$$

  where $\Gamma$ is Gamma function, $\chi_K = \frac{2\pi}{L_0}$ and K is a modified Bessel function of the second kind.

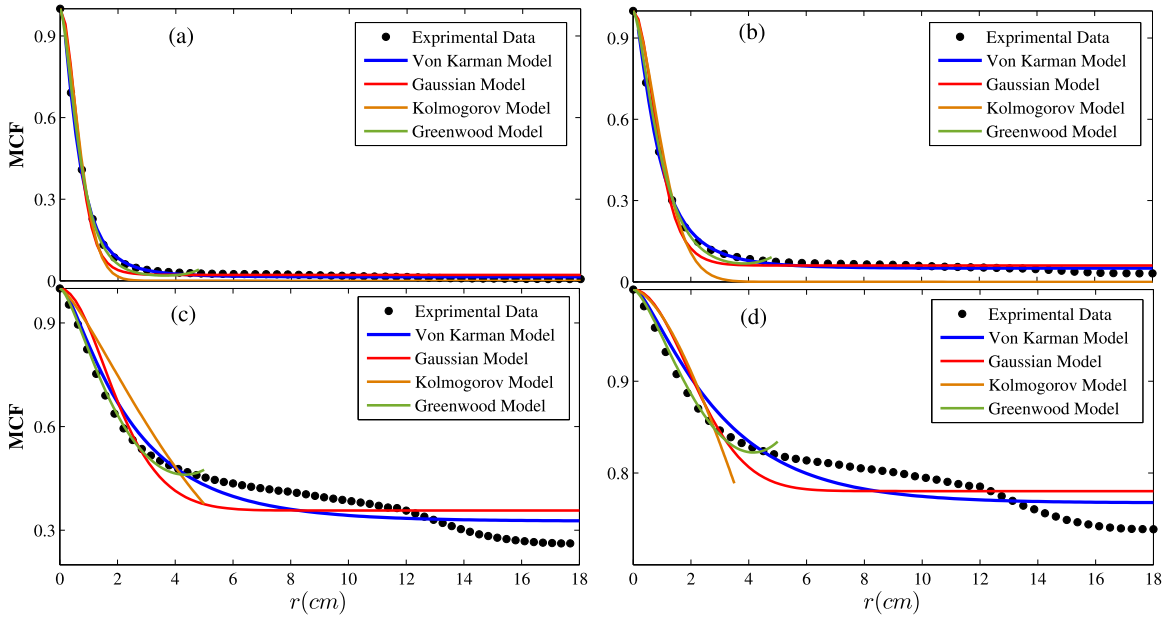


**Fig. 5.** Calculated MCFs from the experimentally measured wavefront gradients, and the different models fitted to the data. The beam path distance from the heater's surface was (a) 13 cm, (b) 30 cm, (c) 80 cm, and (d) 200 cm. The heater temperature was 80 °C .

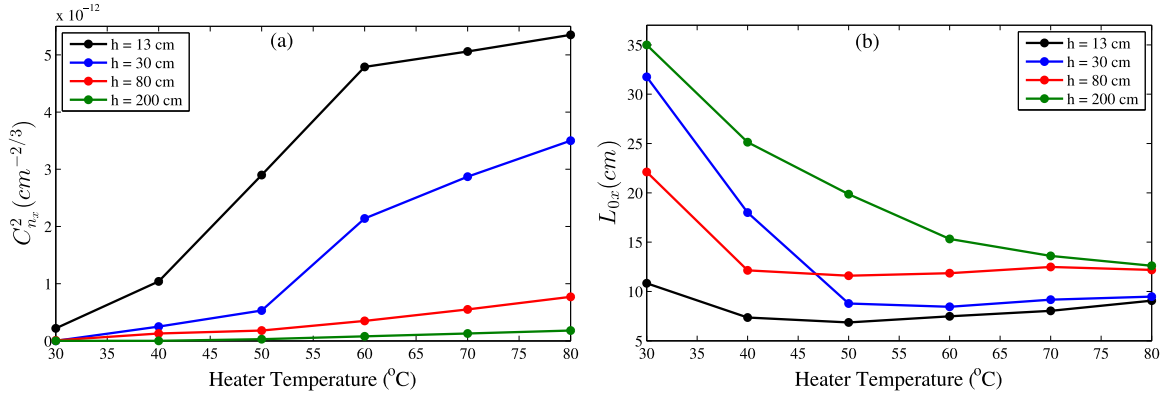


**Fig. 6.** Estimated values of (a) $C_n^2$, and (b) outer scale of the turbulence for different distances of the beam path from the heater surface versus the heater temperature.

- The Greenwood MCF [51]:

$$MCF^{Gr}(r) = exp\left[-\frac{1}{2}\left(6.88(\frac{r}{r_0})^{5/3}{}_2F_3(\frac{11}{12},\frac{17}{12};\frac{11}{6},\frac{11}{6},\frac{1}{2};-\frac{r^2\chi_{Gr}{}^2}{4})\right.\right.$$
$$+32.89(\chi_{Gr}r_0)^{-5/3}\times\left[1-{}_2F_3(\frac{1}{12},\frac{17}{12};\frac{1}{6},-\frac{1}{3},1;-\frac{r^2\chi_{Gr}{}^2}{4})\right]$$
$$-2.27r\chi_{Gr}(\frac{r}{r_0})^{5/3}$$
$$\left.\left.\times{}_2F_3(\frac{17}{12},\frac{23}{12};\frac{7}{3},\frac{7}{3},\frac{3}{2};-\frac{r^2\chi_{Gr}{}^2}{4})\right)\right],$$

where $\chi_{Gr} = 3.349/L_0$ and ${}_pF_q$ is the generalized hypergeometric function.

In Fig. 5 plots show the different models fitted to the experimental MCF values calculated along $x$-direction at different heights of the laser beam path from the heater surface. For all plots, the temperature of the heater was 80 °C. Similarly to Ref. [18], different models were fitted in different ranges to the experimental MCF date. In the fitting process, the Kolmogorov, Gaussian, Greenwood, and von Kármán models were fitted to the experimental data in ranges of 0–2.2 cm, 0–5 cm, 0–5 cm, and 0–10 cm, respectively. By fitting each model over a larger interval, we observed that the mean square error of the corresponding fitting increased significantly. It is worth mentioning that the mean square errors of the fittings in those ranges decrease as the heater temperature increases and the distance of the beam path from the heater decreases.

As can be seen from Fig. 5 and the results of Ref. [18], von Kármán model has the best fit to the experimental PSF and MCF data, because it has the lowest mean square error and is fitted over a larger range than the other models.

Values of turbulence strength, $C_n^2$, and outer scale, $L_0$, for the studied medium at different heater temperatures, and different beam heights from the heater surface are estimated by fitting the von Kármán MCF to the data of Fig. 4, for the horizontal separations of the points. Results are shown in Fig. 6. As is seen, the value of the $C_n^2$ increases by increasing the heater temperature, and it decreases with the height of the beam from the heater. In addition, outer scale decreases by increasing the heater temperature and increasing the height of the beam from the heater.

As mentioned above, Earth atmosphere in the surface layer behaves as a convective turbulence medium. According to the obtained results, for a beam propagating horizontally through this layer, it is expected that its coherence radius significantly reduces when the beam path to be closer to the Earth surface. It is worth mentioning that although PSFs and MCFs, and consequently the coherence radius depend on the beam wavelength, however by using relationships calculated in Ref. [2], the results of this study can be applied to other visible wavelengths and even infrared.

## 4. Conclusion

In this paper, we used a combination of two telescopes and a two-channel moiré deflectometry-based wavefront sensor for estimation of PSF and MCF of a light beam propagates through a convective air turbulence. We also investigated the effects of the different TGs and beam path distances from the heat source on the mentioned functions. It is shown that by increasing the heater temperature, and decreasing the beam path distance from the heater, the PSF increases while MCF decreases. Detail behavior of these functions for different separations of the points on the wavefront were also studied. We also estimated the values of $C_n^2$ and $L_0$ at different conditions. The value of $C_n^2$ increased by increasing the heater temperature, and decreased by increasing the beam path distance from the heater, and $L_0$ decreased by increasing the heater temperature and increasing the beam path distance from the heater.

## Declaration of competing interest

The authors declare that they have no known competing financial interests or personal relationships that could have appeared to influence the work reported in this paper.

## Data availability

Data will be made available on request.

## Acknowledgments

Author Saifollah Rasouli would like to acknowledge Abdus Salam International Center for Theoretical Physics (ICTP), Trieste, Italy, for the Senior Associate Fellowship.

## Funding

Institute for Advanced Studies in Basic Sciences (G2014IASBS12632, G2022IASBS12632).

## References

[1] V.P. Lukin, Investigation of the anisotropy of the atmospheric turbulence spectrum in the low-frequency range, in: Atmospheric Propagation and Remote Sensing IV, Vol. 2471, International Society for Optics and Photonics, 1995, pp. 347–355.
[2] A.S. Gurvich, M.S. Belen'kii, Influence of stratospheric turbulence on infrared imaging, JOSA A 12 (11) (1995) 2517–2522.
[3] E. Golbraikh, N.S. Kopeika, Behavior of structure function of refraction coefficients in different turbulent fields, Appl. Opt. 43 (33) (2004) 6151–6156.
[4] A. Zilberman, E. Golbraikh, N.S. Kopeika, Propagation of electromagnetic waves in Kolmogorov and non-Kolmogorov atmospheric turbulence: three-layer altitude model, Appl. Opt. 47 (34) (2008) 6385–6391.
[5] J. Li, W. Wang, M. Duan, J. Wei, Influence of non-Kolmogorov atmospheric turbulence on the beam quality of vortex beams, Opt. Express 24 (18) (2016) 20413–20423.
[6] L. Cui, B. Xue, X. Cao, F. Zhou, Atmospheric turbulence MTF for optical waves propagation through anisotropic non-Kolmogorov atmospheric turbulence, Opt. Laser Technol. 63 (2014) 70–75.
[7] X. He, B. Lü, Propagation of partially coherent flat-topped vortex beams through non-Kolmogorov atmospheric turbulence, JOSA A 28 (9) (2011) 1941–1948.
[8] M.S. Wei, J. Wang, Y. Zhang, Z.D. Hu, Orbital-angular-momentum photons for optical communication in non-Kolmogorov atmospheric turbulence, Opt. Commun. 416 (2018) 89–93.
[9] C. Rao, W. Jiang, N. Ling, Spatial and temporal characterization of phase fluctuations in non-Kolmogorov atmospheric turbulence, J. Mod. Opt. 47 (6) (2000) 1111–1126.
[10] S. Rasouli, M.D. Niry, Y. Rajabi, A.A. Panahi, J.J. Niemela, Applications of 2-D Moiré deflectometry to atmospheric turbulence, J. Appl. Fluid Mech. 7 (4) (2014).
[11] E.M. Razi, S. Rasouli, Measuring significant inhomogeneity and anisotropy in indoor convective air turbulence in the presence of 2D temperature gradient, J. Opt. 16 (4) (2014) 045705.
[12] S. Rasouli, Y. Rajabi, Investigation of the inhomogeneity of atmospheric turbulence at day and night times, Opt. Laser Technol. 77 (2016) 40–50.
[13] F. Wang, I. Toselli, J. Li, O. Korotkova, Measuring anisotropy ellipse of atmospheric turbulence by intensity correlations of laser light, Opt. Lett. 42 (6) (2017) 1129–1132.
[14] E.M. Razi, S. Rasouli, Impacts of the source temperature and its distance on the statistical behavior of the convective air turbulence, Appl. Phys. B 125 (10) (2019) 1-10.
[15] E.M. Razi, S. Rasouli, Investigation of inhomogeneity and anisotropy in near ground layers of atmospheric air turbulence using image motion monitoring method, Opt. Commun. 383 (2017) 255–259.
[16] I. Stiperski, M. Calaf, Dependence of near-surface similarity scaling on the anisotropy of atmospheric turbulence, Q. J. R. Meteorol. Soc. 144 (712) (2018) 641–657.
[17] E. Mohammadi Razi, S. Rasouli, M. Dashti, J.J. Niemela, A high-resolution wavefront sensing method to investigate the annular Zernike polynomials behaviour in the indoor convective air turbulence in the presence of a 2D temperature gradient, J. Mod. Opt. 68 (18) (2021) 994–1001.
[18] S. Rasouli, R.E. Mohammadi, J.J. Neimela, Investigation of the anisotropy and scaling of the phase structure function in convective air turbulence, J. Opt. Soc. Amer. A 39 (2022) 1–9.
[19] Y. Gu, G. Gbur, Scintillation of Airy beam arrays in atmospheric turbulence, Opt. Lett. 35 (20) (2010) 3456–3458.
[20] Y. Gu, G. Gbur, Scintillation of nonuniformly correlated beams in atmospheric turbulence, Opt. Lett. 38 (9) (2013) 1395–1397.
[21] G.R. Ochs, R.S. Lawrence, Saturation of laser-beam scintillation under conditions of strong atmospheric turbulence, JOSA 59 (2) (1969) 226–227.
[22] Ö.F. Sayan, H. Gerçekçioğlu, Y. Baykal, Hermite Gaussian beam scintillations in weak atmospheric turbulence for aerial vehicle laser communications, Opt. Commun. 458 (2020) 124735.
[23] Ö.F. Sayan, H. Gerçekcioğlu, Y. Baykal, Multimode laser beam scintillations in weak atmospheric turbulence for vertical link laser communications, Waves Random Complex Media (2020) 1–3.
[24] S. Rasouli, M. Dashti, A.N. Ramaprakash, An adjustable, high sensitivity, wide dynamic range two channel wave-front sensor based on moiré deflectometry, Opt. Express 18 (23) (2010) 23906–23915.
[25] M. Dashti, S. Rasouli, Measurement and statistical analysis of the wavefront distortions induced by atmospheric turbulence using two-channel moiré deflectometry, J. Opt. 14 (9) (2012) 095704.
[26] P.P. Andrade, P.J. Garcia, C.M. Correia, J. Kolb, M.I. Carvalho, Estimation of atmospheric turbulence parameters from Shack–Hartmann wavefront sensor measurements, Mon. Not. R. Astron. Soc. 483 (1) (2019) 1192–1201.
[27] S. Ding, R. Li, Y. Luo, A. Dang, Polarization coherent optical communications with adaptive polarization control over atmospheric turbulence, JOSA A 35 (7) (2018) 1204–1211.
[28] Y. Wang, F. Du, J. Ma, L. Tan, Employing circle polarization shift keying in free space optical communication with gamma–gamma atmospheric turbulence channel, Opt. Commun. 333 (2014) 167–174.
[29] G. Wu, B. Luo, S. Yu, A. Dang, T. Zhao, H. Guo, Effects of coherence and polarization on the beam spreading and direction through atmospheric turbulence, Opt. Commun. 284 (19) (2011) 4275–4278.
[30] C. Luo, X.E. Han, Evolution and Beam spreading of arbitrary order vortex beam propagating in atmospheric turbulence, Opt. Commun. 460 (2020) 124888.
[31] G. Wu, H. Guo, S. Yu, B. Luo, Spreading and direction of Gaussian–Schell model beam through a non-Kolmogorov turbulence, Opt. Lett. 35 (5) (2010) 715–717.
[32] W. Du, H. Zhu, D. Liu, Z. Yao, C. Cai, X. Du, R. Ai, Effect of non-Kolmogorov turbulence on beam spreading in satellite laser communication, J. Russ. Laser Res. 33 (5) (2012) 456–463.
[33] P. Barcik, L. Hudcova, Measurement of spatial coherence of light propagating in a turbulent atmosphere, Radioengineering 22 (1) (2013) 341–345.
[34] W. Sheng, Y. Su-Hui, W. Xia, Z. Chang-Ming, Z. Qi-Hai, Experimental study on influence of atmospheric turbulence on coherence of dual-frequency laser, Chin. Phys. Lett. 27 (8) (2010) 084202.
[35] W. Gao, Change of coherence of light produced by tissue turbulence, J. Quant. Spectrosc. Radiat. Transfer 131 (2013) 52–58.
[36] W. Gao, O. Korotkova, Changes in the state of polarization of a random electromagnetic beam propagating through tissue, Opt. Commun. 270 (2) (2007) 474–478.
[37] M. Born, E. Wolf, Principle of Optics, Cambridge University, 1999.
[38] F. Wang, X. Liu, Y. Cai, Propagation of partially coherent beam in turbulent atmosphere: a review (invited review), Prog. Electromagn. Res. 150 (2015) 123–143.
[39] Z. Liu, D. Zhao, Propagation of partially coherent vortex beams in atmospheric turbulence by a spatial light modulator, Laser Phys. Lett. 16 (5) (2019) 056003.
[40] J.K. Jabczyński, P. Gontar, Impact of atmospheric turbulence on coherent beam combining for laser weapon systems, Def. Technol. 17 (4) (2021) 1160–1167.
[41] Y. Li, M. Gao, H. Lv, L.G. Wang, Statistical properties of a return wave generated from an arbitrary rough target in atmospheric turbulence by a partially coherent beam with radial polarization, J. Mod. Opt. 68 (2) (2021) 72–86.

[42] Y. Li, M. Gao, H. Lv, L. Wang, B. Li, S. Ren, P. Wu, Statistical properties of a spatiotemporally partially coherent vector cosine-Gaussian-correlated pulsed beam with radial polarization in atmospheric turbulence, Waves Random Complex Media (2021) 1–23.
[43] L. Zhao, Y. Xu, Y. Dan, Evolution properties of partially coherent radially polarized Laguerre–Gaussian vortex beams in an anisotropic turbulent atmosphere, Opt. Express 29 (22) (2021) 34986–35002.
[44] L. Mandel, E. Wolf, Optical Coherence and Quantum Optics, Cambridge university press, 1995.
[45] M. Panahi, R. Shomali, M. Mollabashi, Use of a 4-aperture DIMM instrument for atmospheric coherence time estimation: an analytical development, JOSA A 36 (4) (2019) 655–664.
[46] B. Schäfer, K. Mann, Determination of beam parameters and coherence properties of laser radiation by use of an extended Hartmann-Shack wave-front sensor, Appl. Opt. 41 (15) (2002) 2809–2817.
[47] R.V. Shack, Production and use of a lecticular hartmann screen, J. Opt. Soc. Amer. 61 (1971) 656–661.
[48] M. Yeganeh, S. Rasouli, M. Dashti, S. Slussarenko, E. Santamato, E. Karimi, Reconstructing the Poynting vector skew angle and wavefront of optical vortex beams via two-channel moiré deflectometery, Opt. Lett. 38 (6) (2013) 887–889.
[49] F. Roddier, Adaptive Optics in Astronomy, Cambrige University Press, 1999.
[50] A. Consortini, L. Ronchi, Choice of the model of atmospheric turbulence, Appl. Opt. 11 (5) (1972) 1205–1211.
[51] V.V. Voitsekhovich, Outer scale of turbulence: comparison of different models, JOSA A 12 (6) (1995) 1346–1353.